Science of the Total Environment 880 (2023) 163289

Contents lists available at ScienceDirect

Science of the Total Environment

journal homepage: www.elsevier.com/locate/scitotenv

Improving accuracy of quantifying nitrate removal performance and enhancing understanding of processes in woodchip bioreactors using high-frequency data

A. Rivas [a,*], G. Barkle [b], T. Sarris [c], J. Park [a], A. Kenny [c], B. Maxwell [d], R. Stenger [a], B. Moorhead [a], L. Schipper [e], J. Clague [a]

[a] Lincoln Agritech Ltd., Private Bag 3062, Hamilton 3240, New Zealand
[b] Land and Water Research Ltd., PO Box 27046, Garnett Ave., Hamilton 3257, New Zealand
[c] Institute of Environmental Science and Research, PO Box 29-181, Christchurch 8540, New Zealand
[d] Department of Crop Sciences, University of Illinois Urbana-Champaign, Urbana, IL 61801-4730, USA
[e] University of Waikato, Private Bag 3105, Hamilton 3240, New Zealand

HIGHLIGHTS

- A robust method for accounting lag time in bioreactors using high-frequency data is introduced.
- Greater removal rates were calculated using high-frequency data than with low-frequency data.
- Nitrate loading and electron donor availability influenced variability in removal processes within the bioreactor.
- Michaelis-Menten kinetics can describe the nitrate dynamics in woodchip bioreactor.
- Designing bioreactors needs to balance volumetric efficiency and avoid strongly reducing conditions.

GRAPHICAL ABSTRACT

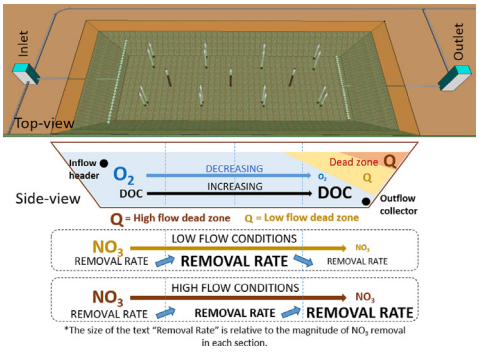

ARTICLE INFO

Editor: Jan Vymazal

Keywords:
High-frequency monitoring
Lag time
Nitrogen
Volumetric efficiency
Michaelis-Menten kinetics
Drainage

ABSTRACT

Woodchip bioreactors have gained popularity in many countries as a conservation practice for reducing nitrate load to freshwater. However, current methods for assessing their performance may be inadequate when nitrate removal rates (RR) are determined from low-frequency (e.g., weekly) concurrent sampling at the inlet and outlet. We hypothesised that high-frequency monitoring data at multiple locations can help improve the accuracy of quantifying nitrate removal performance, enhance the understanding of processes occurring within a bioreactor, and therefore improve the design practice for bioreactors. Accordingly, the objectives of this study were to compare RRs calculated using high- and low-frequency sampling and assess the spatiotemporal variability of the nitrate removal within a bioreactor to unravel the processes occurring within a bioreactor. For two drainage seasons, we monitored nitrate concentrations at 21 locations on an hourly or two-hourly basis within a pilot-scale woodchip bioreactor in Tatuanui, New Zealand. A novel method was developed to account for the variable lag time between entry and exit of a parcel of sampled drainage water. Our results showed that this method not only enabled lag time to be accounted for but also helped quantify volumetric inefficiencies (e.g., dead zone) within the bioreactor. The average RR calculated using this method was significantly higher than the average RR calculated using conventional low-frequency methods. The average RRs of each of the quarter sections within the bioreactor were found to be different. 1-D transport modelling confirmed the effect of nitrate loading on the removal process as nitrate reduction followed Michaelis-Menten (MM) kinetics. These results

* Corresponding author.
E-mail address: aldrin.rivas@lincolnagritech.co.nz (A. Rivas).

http://dx.doi.org/10.1016/j.scitotenv.2023.163289
Received 28 June 2022; Received in revised form 15 March 2023; Accepted 31 March 2023
Available online 5 April 2023

demonstrate that high-frequency temporal and spatial monitoring of nitrate concentrations in the field allows improved description of bioreactor performance and better understanding of processes occurring within woodchip bioreactors. Thus, insights gained from this study can be used to optimise the design of future field bioreactors.

1. Introduction

Woodchip bioreactors have been gaining popularity in many countries as a conservation practice for reducing nitrate load to receiving waters due to their simplicity, low maintenance requirements and costs, and reasonable efficiency of nitrate removal (Christianson et al., 2021). Woodchip bioreactors have been shown to be effective in removing nitrate from artificial drainage, with reported removal efficiencies of between 12 and 99 % of the input load (Jaynes et al., 2008; Christianson et al., 2012; Hassanpour et al., 2017). However, current methods for assessing performance of field bioreactors may be inaccurate, as nitrate removal rates (RR) and efficiencies (RE) are generally determined from low-frequency concurrent sampling (e.g., weekly) at the inlet and outlet (Schipper et al., 2010a; Rivas et al., 2020b). With inputs (flow and nitrate concentrations) to the bioreactors being typically variable in response to changing weather conditions, output concentrations do not necessarily correspond well with input concentrations measured concurrently, i.e., at the same time. Such input/output sampling methods also essentially treat bioreactors as "black boxes" and cannot consider variation in RR within the bioreactors, in time and space (Christianson et al., 2012; Hassanpour et al., 2017; Husk et al., 2017). Obtaining a clearer understanding of how the attenuation processes progress within bioreactors at varying flow rates and nitrate concentrations would help to improve their design.

The common measures used to assess the performance of woodchip bioreactors in the field are nitrate RE and RR. RE is the percentage of the nitrate load that was removed from the drainage water being treated over a defined period (Christianson et al., 2012), typically a drainage season. RE varies substantially between periods, depending on the inflow and nitrate dynamics (Rivas et al., 2020b). Whereas RR, which is the focus of this study, is the amount of nitrate removed per unit volume of the bioreactor per unit time and is a design characteristic more attributable to the substrate (and age) used in the bioreactor (Christianson et al., 2012; Rivas et al., 2020b). There are two widely adopted methods for calculating RR: 1) cumulative RR over a relatively longer time period (e.g., three months to seasonal), in which RR is computed from the difference between the nitrate load and the discharge (inflow mass – outflow mass) over the time period divided by the saturated volume (Maxwell et al., 2020; Rivas et al., 2020b) or the total volume of the bioreactor (Christianson et al., 2012); and 2) concurrent RR (also called instantaneous RR; Maxwell et al. (2020)), where the mass of nitrate removed is calculated from pairs of concurrently measured nitrate concentrations at the inlet and outlet, multiplied by the instantaneous flow rate at the time of the measurement, and divided by the saturated volume (Ghane et al., 2015; Maxwell et al., 2020; Manca et al., 2021) or the total volume of the bioreactor (Schipper et al., 2010a; Warneke et al., 2011a; Christianson et al., 2013; Lepine et al., 2016). The limitations of cumulative RR method are: having only one averaged value for the season (or more, but still limited values if the drainage season is separated into several periods), and inability to determine the temporal changes in RR over the calculation period. The concurrent RR method disregards that the water being sampled concurrently at the inlet and outlet are not consistently related due to variation in flow rates and nitrate concentrations between when the sampled water enters and discharges. This lag time between entry and exit is problematic for the calculation of RR using the concurrent method, as drainage flow rates and nitrate concentrations are temporally variable as observed in New Zealand and many other temperate countries (Barkle et al., 2021).

Optical nitrate sensors provide an excellent opportunity for cost-effective monitoring of nitrate at multiple locations and at high frequency (Etheridge et al., 2014; Birgand et al., 2016; Maxwell et al., 2018; Liu et al., 2020b). A number of hydrological studies have demonstrated that high-frequency monitoring of nitrate in tile drains and rivers improves the accuracy of load estimates and can better reveal the dynamics (Liu et al., 2020b). For instance, in a study on tile drained landscapes which found that nitrate concentrations should be determined every 3–18 days to keep load estimates within 10 % of reference loads, Williams et al. (2015) used sub-daily (2–4 h) intervals during storm events at some sites, and other sites were sampled daily and the daily concentrations were interpolated to estimate hourly nitrate concentrations at other sites. A study comparing different sampling frequencies for calculating nitrate loads from subsurface drains showed weekly sampling provided load estimates within 15 % of 'true' load using daily sampling (Wang et al., 2003). However, the study computed nitrate loads at a single point only as compared to the two points necessary for determining RR in woodchip bioreactors wherein accounting for lag time is deemed essential, especially for highly dynamic drainage flows.

However, few field bioreactor studies have utilised high-frequency monitoring. Maxwell et al. (2020) reported that hourly monitoring identified significant lag in nitrate concentrations between inlet and outlet, and therefore concluded that inaccuracies will occur when estimating RR using concurrent measurement methods. They also reported preferential flows and dead spots within a bioreactor (Maxwell et al., 2020). Utilising high-frequency sampling during storm events (2-h composites of four 30-min samplings; sampling for 48 h. per storm), Pluer et al. (2019) found that RR was higher during storm flow than during baseflow. In comparing RR calculations that used lag time to match parcels (based on theoretical hydraulic retention time using pore volume estimates) with concurrent sampling (bi-weekly), they also found that the lag time-matched parcels produced RR results that were significantly lower (Pluer et al., 2019). These studies demonstrate the need to better understand the spatial and temporal variability of nitrate removal within the bioreactor and the factors affecting this variability. Information on the changes in nitrate along the length of a bioreactor provides a better understanding of how bioreactors work and can reveal opportunities for improving their design and performance. We hypothesised that high-frequency monitoring at multiple locations within a bioreactor, especially for systems with highly dynamic flows, can help improve the accuracy of quantifying the nitrate removal performance of woodchip bioreactors and enhance our understanding of processes occurring within a bioreactor. Therefore, the three main objectives of this research were to: 1) introduce a robust approach to account for the variable lag times between entry and exit when calculating nitrate loads and RRs in woodchip bioreactors; 2) compare RRs obtained using high-frequency and lower-frequency sampling; and 3) assess the spatiotemporal variability of the nitrate removal within a bioreactor.

2. Methods and materials

2.1. Study site

This research was conducted at a pilot-scale woodchip bioreactor installed in 2017 on a pastoral dairy farm near Tatuanui in the Waikato region, New Zealand. The lined bioreactor is trapezoidal in shape and filled with *Pinus radiata* (Monterey pine) woodchips (Fig. 1). It receives artificial drainage from an area of approx. 0.65 ha. The bioreactor was sized to remove approximately 50 % of estimated annual nitrate load based on limited data of highly variable flow and nitrate concentrations. Using a flow duration curve, we determined the target flow rate for the corresponding 50 % of the annual load. Then assuming an average nitrate concentration based on our limited data, we determined the target load. Accordingly, using this target load (in g-N day^{-1}) and an assumed nitrate removal rate of

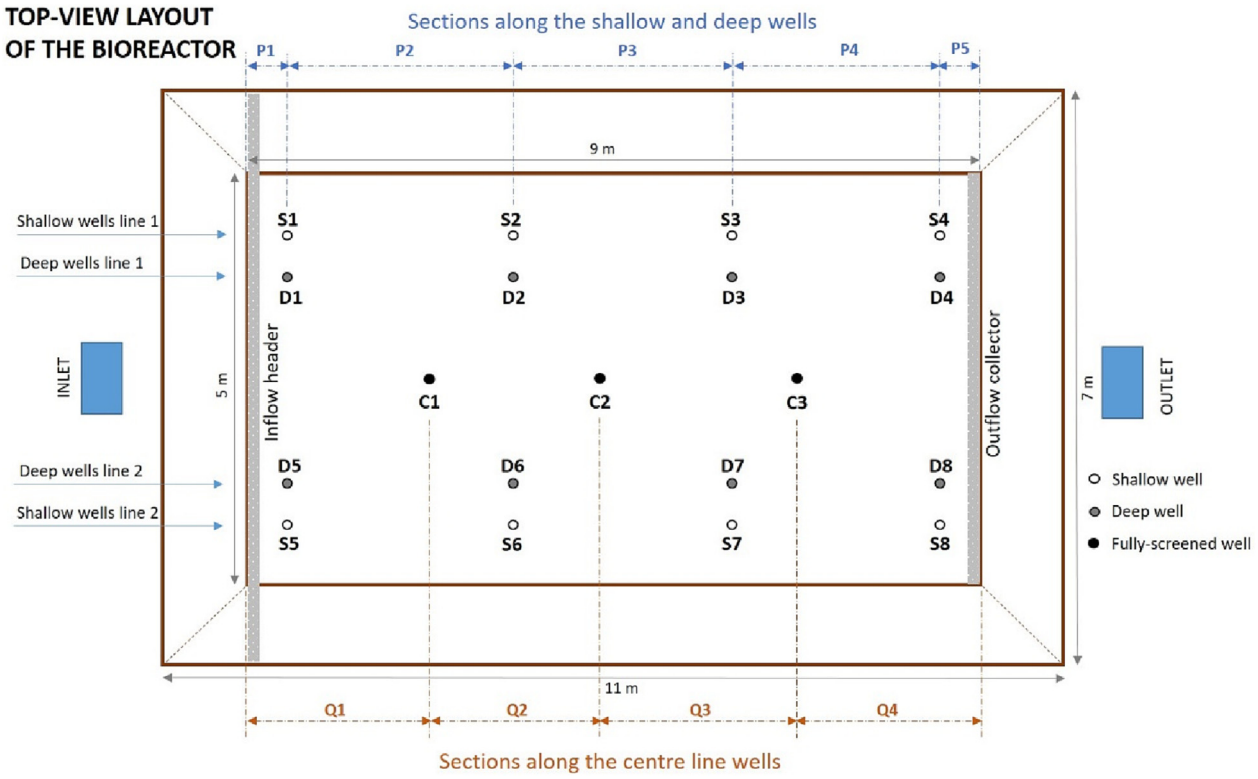

Fig. 1. Layout of the Tatuanui woodchip bioreactor showing the monitoring wells from which water was drawn for high-frequency measurements of nitrate. Flow direction is from left to right.

3.5 g-N m^{-3} day^{-1} (Cameron and Schipper, 2012), we calculated the required volume of the bioreactor. The bioreactor inlet has a perforated pipe installed across the width of the bioreactor, perpendicular to the flow direction at about 0.8 m above the floor of the bioreactor. The perforated pipe is a twin wall polyethylene pipe with smooth inner wall (Iplex NexusFlo) and inside diameter of approx. 100 mm. The total area of roughly rectangular perforations (1.5 mm by 14 mm) is around 6 % of wall surface area. The outflow was collected from a similar perforated drainage pipe on the bioreactor floor near the outlet as shown in Fig. 1. The depth of the water table above the bioreactor floor was controlled by the height of the outlet V-notch weir where the outflow was also being measured. Due to minor changes in the inflow and outflow configuration, the saturated depth at no flow was 0.939 m and 0.834 during the 2018 and 2019 seasons, respectively. More detailed information about the Tatuanui bioreactor is provided by Rivas et al. (2020b).

To monitor nitrate concentrations at different locations through the bioreactor, 19 wells were installed within the bioreactor in the later part of the 2018 drainage season (Fig. 1). Three fully screened wells over the entire saturated depth were installed approximately at equidistance along the centreline of the bioreactor, with four sets of paired shallow and deep wells installed along both sides of the bioreactor. The shallow wells were screened (0.10 m long) at 0.6–0.7 m above the bioreactor floor, while the deep wells were screened at 0.3–0.4 m above the floor.

2.2. Multiplexer sampling and nitrate measurement with optical sensor

This study employed a multiplexer and a spectrophotometer (spectro::lyser, s::can GmbH, Vienna, Austria) for each longitudinal half of the bioreactor for a one-month sampling period in the later part of the 2018 drainage season (8 Aug to 8 Sep 2018; late winter to early spring). Thus, the high-frequency monitoring presented in this study covered a portion only of the entire 2018 drainage season (25 May–11 Sep 2018; SF10a). This multiplex sampling system is described in detail by Maxwell et al. (2020). Briefly, pore water samples were collected sequentially from all the wells including the Inlet and Outlet on approximately a one-hour basis. Throughout the 2019 drainage season, high-frequency monitoring was carried out from 9 Aug to 26 Oct (late winter to mid-spring; SF10b). The monitoring data from the later part of 2019 season (from noon of 3rd Oct 2019; SF10b) were excluded as a preliminary investigation of supplemental carbon dosing was conducted during this period. Due to the unavailability of the multiplexer and optical sensors used in the 2018 season, a slightly different multiplex system sampled and measured nitrate-nitrogen (NO_3^--N) concentrations at the Inlet, Outlet and all 19 wells using: a peristaltic pump (set at approx. 60 mL/min); solenoid valves (12v 5.5W) and logger (CR1000, Campbell Scientific) to control the opening of valves for selecting the specific location to be sampled; and an optical sensor (OPUS, TriOS, Rastede, Germany). A custom-designed, 3D-printed silver-coated PVC insert was fitted into the flow cell of the sensor to minimise the volume of water required to flush the system (from approx. 33 mL to 5–6 mL) at each sampling. After each complete cycle of all locations, taking about 2 h, the probe was flushed for 60 s with deionised water to ensure sufficient flushing of the probe (Liu et al., 2020a). The probe was cleaned regularly (approximately every two weeks or more frequently as required) based on monitored absorbance readings.

For both 2018 and 2019 sampling campaigns, sensor readings were post-calibrated with NO_3^--N concentrations measured in the laboratory. Details on the probe calibration for the 2018 season have been reported (Maxwell et al., 2020). In the 2019 season, two sampling campaigns were conducted in September 2019 to obtain data for the post-calibration of the optical sensor NO_3^--N data. Samples for laboratory analysis were collected from the outflow of the optical sensor to ensure NO_3^--N concentration was measured on the same sampled water. A total of 20 samples originating from various locations (from the Inlet to the Outlet) in the bioreactor were collected and transported in a cooler with ice pack and kept in the fridge at <4 °C until submitted within 24 h to Analytica Laboratories Ltd. in Hamilton, New Zealand for analysis. NO_3^--N in samples was measured colourimetrically by flow injection analysis (following APHA NO_3-I. Online edition). The range in NO_3^--N concentrations for this calibration

campaign was ~1 to 15 mg-N L^{-1} with a very high correlation in NO_3^--N measured by the optical sensor and the laboratory obtained (R^2 = 0.998). Using the linear regression between the two methods for measuring NO_3^--N concentrations (Maxwell et al., 2020), NO_3^--N readings of the optical sensor were post-calibrated and used in the analysis.

In addition to the NO_3^--N sensor measurements, 500 mL of drainage water was sampled at the Inlet and Outlet every 10 m^3 of flow using an autosampler (ISCO 3700, Teledyne ISCO, Lincoln NE, USA) during both seasons. Water samples were also collected manually on a weekly to fortnightly basis from the Inlet, Outlet, and middle well C2 and analysed for NO_3^--N and dissolved organic carbon (DOC). Details on the sampling methods have been described (Rivas et al., 2020b). Samples were analysed for NO_3^--N using a flow injection analyser following APHA 4500 at the NIWA laboratory, Hamilton, NZ, whereas DOC was measured at the Eurofins ELS Ltd. laboratory in Lower Hutt, NZ following APHA 5310 (B, C) (Rice et al., 2012).

2.3. Novel approach to account for lag time in woodchip bioreactors

In this study, we developed a method for calculating nitrate removal rate (RR) that considers the lag time required for a parcel of water to move from the Inlet to the Outlet and to sampling points through the bioreactor. Several studies (e.g., Pluer et al. (2019)) have accounted for this lag assuming piston flow characteristics, in which the lag time was based on theoretical values of hydraulic residence time (or theoretical HRT) using estimated or measured total pore volume and flow (Kadlec and Wallace, 2009; Ghane et al., 2019). However, other studies have concluded that this assumption of using the theoretical HRT fails to account for non-uniform flow and possible no flow or dead flow zones (Cameron and Schipper, 2011; Christianson et al., 2013; Jaynes et al., 2016). Tracer studies can provide estimates of actual HRT (Ghane et al., 2019), which may be calculated using drainable porosity (Ghane et al., 2016). However, tracer studies were usually undertaken under steady flow conditions or with individual pulse events (Christianson et al., 2013). In bioreactors with highly variable flows, conducting multiple conservative tracer tests to determine HRT covering the variable natural flow rates is extremely challenging. The alternative is to use obvious break points in the NO_3^--N concentration to determine the lag time, though this method had only been applied in a limited manner (i.e., for verifying theoretical HRT) to monitoring data of short duration (48-h) storm events (Pluer et al., 2019).

In this study, our method for accounting lag time was based on volumetric efficiency. Volumetric efficiency is defined as the ratio of mean tracer HRT (or actual HRT) to the theoretical HRT (Thackston et al., 1987; Kadlec and Wallace, 2009; Cameron and Schipper, 2012; Christianson et al., 2013), the latter being based on total pore volume estimates (Kadlec and Wallace, 2009; Christianson et al., 2013; Ghane et al., 2019). This definition is applicable for tracer tests with a pulse of tracer and tracer recovery is measured to estimate effective porosity (or drainable porosity). In the approach developed in this paper, we matched natural NO_3^--N peaks as a tracer in the drainage flow through the bioreactor to estimate the effective pore volumes between different measurement points through the bioreactor. We then determined the volumetric efficiency based on the ratio of time between peaks to the theoretical HRT. This approach took inspiration from the method developed by Persson et al. (1999) using the ratio of 'time to peak' in tracers to theoretical HRT to understand flow dynamics in wetlands, and the use of concentration break points for determining HRT by Pluer et al. (2019). We focused on discernible NO_3^--N concentration peaks travelling from the Inlet to the Outlet along the length of the bioreactor as monitored by wells within the bioreactor. The availability of high-frequency data is essential for the feasibility of this method, due to the required confidence in determining the time for a NO_3^--N concentration peak to travel from one monitoring location to the next ('time between peaks'). This method would be unlikely to be feasible with low-frequency measurements as the peak of NO_3^--N concentrations would be missed. We used a total porosity of 0.86 determined in the laboratory using woodchips from the same supplier with similar drainable porosity (0.49 in the lab vs 0.45–0.50 determined in the field). This total porosity falls within the range of values (0.83–0.86) determined from old and fresh woodchips by Ghane et al. (2014).

The detailed procedure for accounting the lag time ("Matched Parcels" method) and calculating nitrate removal rate is presented in the Supplementary Materials (SM1). This procedure was applied to NO_3^--N concentration data collected from the Inlet, the wells in the centreline, and the Outlet enabling the analysis to investigate the different quarter sections of the bioreactor, namely the first (Q1), middle (Q2 + Q3) and last (Q4) quarter sections. As discussed below (Section 3.1.2), the NO_3^--N concentrations in well C2 were excluded, resulting in the middle section being Q2 + Q3. These data were considered sufficient to investigate and demonstrate the benefits of using high-frequency data in terms of improvement in the estimates of nitrate removal compared with using low-frequency concurrent data, as well as determine new insights on removal processes occurring in the bioreactor. To additionally investigate the spatial variability in the nitrate removal performance across all monitored locations, i.e., laterally across, and at upper and lower depths of the bioreactor, as well as the centreline wells, a reactive transport simulation model was applied, as described in the following section.

2.4. Using reactive transport modelling to investigate the spatially variable nitrate removal rate

Bioreactor designs frequently rely on uniform removal rates (RR) to predict performance and nitrate removal. Design RRs are often adjusted for temperature (Sarris and Burbery, 2018 and references therein) or nitrate limiting conditions (Kouanda and Hua, 2021). Here, we inverted a nitrate transport model to derive a) the spatially distributed RRs at various bioreactor sections that best fit the high-frequency monitoring data using zero-order kinetics model, and b) the maximum nitrate removal rates (V_{max}) across the bioreactor, using a Michaelis-Menten (MM) kinetics model to account for nitrate limiting conditions (Ghane et al., 2015).

The transient fate and transport of nitrate in Fickian, porous media with no internal sources and sinks can be expressed as (Zheng and Wang, 1999; Sarris et al., 2018):

$$\frac{\partial(\theta C)}{\partial t} = \nabla\cdot(\theta D\cdot\nabla C) - \nabla\cdot(\theta v_i C) + \Sigma R \tag{1}$$

where C is the NO_3^--N concentration; θ is the dimensionless porosity of the bioreactor medium; D is the hydrodynamic dispersion coefficient tensor defined as the sum of the mechanical dispersion coefficient tensor and molecular diffusion coefficient; v_i is the linear pore water velocity. ΣR is the chemical reactions term used to include the effect of all biochemical and geochemical reactions, which for zero-order reaction kinetics, reduces to the nitrate removal rate of the bioreactor or the bioreactor section. Zero-order kinetic model has been found appropriate for predicting removal rate in woodchip bioreactors when NO_3^--N concentrations were above 2 mg L^{-1} (Halaburka et al., 2017). Our NO_3^--N data at entries of sections investigated were generally above 2 mg L^{-1}, despite periods of nitrate limited conditions. For one-dimensional flow along a flowline, and by ignoring dispersion effects, the explicit forward finite difference solution of (1) becomes:

$$C_{i,t} = C_{i,t-\Delta t} + v\Delta t\,\frac{C_{i-\Delta x,t} - C_{i,t-\Delta t}}{\Delta x} - \frac{k_i\,\Delta t}{\theta} \tag{2}$$

In (2), $C_{i,t}$ is the NO_3^--N concentration in point i and time t; Δx and Δt are the space and time discretisation intervals. For zero-order kinetics, k_i is the uniform nitrate removal rate between $i - \Delta x$ and i. For the Michaelis-Menten kinetics model, k_i becomes:

$$k_i = V_{max}\frac{C_{i,t-\Delta t}}{K_m + C_{i,t-\Delta t}} \tag{3}$$

where V_{max} is the uniform maximum removal rate, and is K_m is the uniform half saturation constant (Kouanda and Hua, 2021). For the Tatuanui bioreactor, the 1D nitrate transport model as shown in Eq. (2) was solved

analytically for the period between 8 Aug 2018 to 8 Sept 2018 and between 15 Aug 2019 to 10 Sep 2019, avoiding periods of no and very low-flow. The flow through the bioreactor was assumed to be represented by five parallel one-dimensional flowlines along the bioreactor length (shallow well lines 1 and 2, deep well lines 1 and 2 and centreline) corresponding to the monitoring arrays (Fig. 1). Shallow well lines 1 and 2 refer to the flowlines on the left (S1–S4) and the right sides (S5–S8), respectively. Deep well lines 1 and 2 refer also to the flowlines on the left (D1–D4) and right edges (D5–D8), respectively. Centreline refers to the flowline along C1–C3. The transient travel distances between all sequential observation points were estimated using MODPATH (Pollock, 1994), and were used for the calculation of residence times in each bioreactor section. The boundary inlet and outlet NO_3^--N concentrations have been linearly interpolated between two hourly measurement times to correspond to a five-minute model time discretisation. The simulation method also permitted the 1D model to use simulated NO_3^--N concentrations for the missing data at well C2 to determine k at middle sections Q2 and Q3 (Fig. 1), even though we discarded the NO_3^--N data at well C2 (see Section 3.1.2). The spatially variable k_i and the uniform V_{max} and K_m, were calibrated in each flowline independently, so that the normalised mean squared error (nRMSE) between simulated and observed NO_3^--N concentrations along each flowline is minimised. In recognition of the different flow and loading characteristics between the two drainage years, k_i and V_{max} have been calibrated for each year, while K_m has been assumed constant in time and calibrated for the nitrate limited 2018 season.

2.5. Statistical analysis

The results, e.g. removal rates, were assessed for normality using the Shapiro-Wilk test (Helsel and Hirsch, 2002), the Kolmogorov-Smirnov test (Daughney and Reeves, 2005), as well as Fisher's measure of skewness (Ghasemi and Zahediasl, 2012) using IBM SPSS Statistics 29. The results were considered to be normally distributed if at least one of the tests was satisfied (Rivas et al., 2017). When required, the results were log-transformed to achieve normal distribution. We used the Levene's test using IBM SPSS Statistics 29 to assess the homogeneity of variance. Considering that we were dealing with time series data, we assessed the data for autocorrelation before performing comparative analysis (Zwiers and von Storch, 1995; O'Shaughnessy and Cavanaugh, 2015). To account for autocorrelation, we first determined the equivalent sample size, then performed *t-test* compensating for autocorrelation (Zwiers and von Storch, 1995; O'Shaughnessy and Cavanaugh, 2015). In comparing three or more groups of data (e.g., removal rates), we assessed first if at least one group significantly differs from the others using *t-test* with the Holm-Bonferroni correction (Holm, 1979). The assessment for autocorrelation and comparative analyses using *t-test*, along with regression analysis, were completed in MS Excel.

3. Results

The Tatuanui bioreactor received highly variable flows and NO_3^--N concentrations in both monitored periods. Flows during the monitored part of the 2018 season varied between 1.5 and 9.4 L min^{-1} (Fig. 2a, supplementary Table ST1); whereas NO_3^--N concentrations varied between 6.1 and 9.5 mg L^{-1} (Table 1, Fig. 2a). In the 2019 season lasting for approximately three months, flow ranged between 0 and 18.7 L min^{-1} (Fig. 3a, supplementary ST1), whereas NO_3^--N concentrations ranged between 10.5 and 36.4 mg L^{-1} (Table 2).

The effect of temperature on nitrate removal was not considered necessary in this study given the relatively stable temperature of the inflow

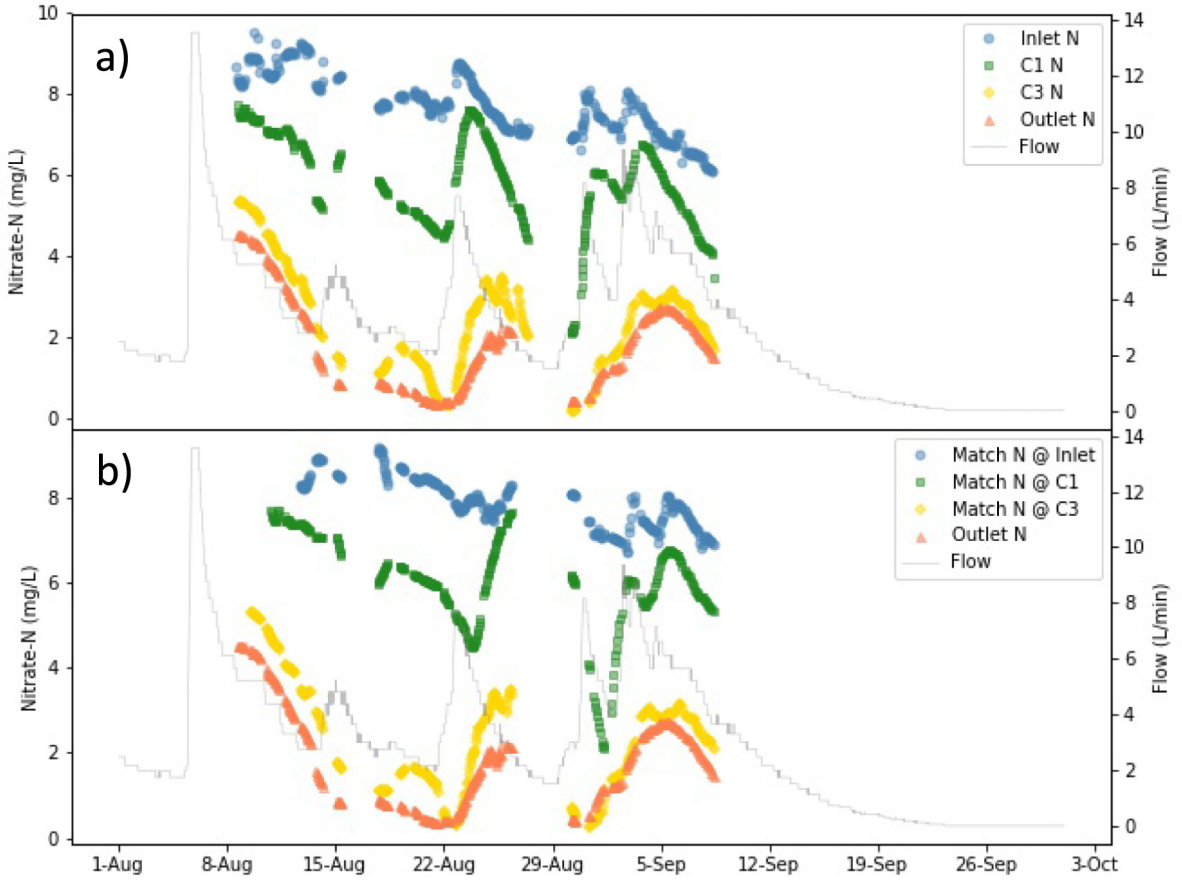

Fig. 2. Time series of nitrate concentrations at different locations along the length of the Tatuanui bioreactor a) as measured by the sensor, and b) lag time-adjusted (except outlet concentrations) during the latter part of the 2018 drainage season.

Table 1
Descriptive statistics of nitrate-N concentrations (mg L^{-1}) at different locations in the Tatuanui bioreactor, a) as measured by the sensor and b) matched or lag time-adjusted, during the partial 2018 drainage season. Frequency of measurements was approximately 1 h.

a) Nitrate-N concentrations (mg L^{-1}) as measured by the sensor

Statistic	Inlet	C1	C3	Outlet
Mean	7.78	5.86	2.48	1.88
Median	7.74	5.89	2.61	1.82
Max	9.52	7.73	5.38	4.53
Min	6.08	2.09	0.19	0.35
Stdev	0.76	1.18	1.27	1.19

b) Lag time-adjusted nitrate-N concentrations (mg L^{-1}) (except outlet)

Statistic	Matched Inlet	Matched C1	Matched C3	Outlet
Mean	7.90	6.03	2.43	1.88
Median	7.91	6.07	2.57	1.82
Max	9.15	7.70	5.32	4.53
Min	6.73	2.12	0.29	0.35
Stdev	0.57	1.11	1.31	1.19

Table 2
Descriptive statistics of nitrate-N concentrations (mg L^{-1}) at different locations in the Tatuanui bioreactor, a) as measured by the sensor and b) matched or lag time-adjusted, during the 2019 drainage season. Frequency of measurements was approximately 2 h.

a) Nitrate-N concentrations (mg L^{-1}) as measured by the sensor

Statistic	Inlet	C1	C3	Outlet
Mean	19.01	16.16	14.51	13.75
Median	18.68	16.99	14.67	13.89
Max	36.39	33.10	30.68	25.27
Min	10.47	0.00	0.00	0.00
Stdev	5.82	7.97	7.54	6.65

b) Lag time-adjusted nitrate-N concentrations (mg L^{-1}) (except outlet)

Statistic	Matched inlet	Matched C1	Matched C3	Outlet
Mean	21.36	19.93	15.48	13.75
Median	22.27	20.30	15.91	13.89
Max	36.13	33.07	30.66	25.27
Min	11.01	10.91	0.00	0.00
Stdev	5.58	5.64	6.82	6.65

drainage water during the study periods (mean ± stdev): 12.3 ± 0.8 °C and 12.6 ± 0.7 °C in the 2018 and 2019 periods, respectively (ST1). The reported factor of increase in the nitrate RR with every 10 °C rise in temperature (i.e., Q_{10}) ranges between 1.2 and 3.8 for investigated temperatures ranging from 5 to 27 °C (Elgood et al., 2010; Warneke et al., 2011b; Warneke et al., 2011c; David et al., 2016). Thus, no substantial effect of temperature is expected on nitrate removal performance of the Tatuanui bioreactor due to the small difference in the inflow temperature between and within seasons.

3.1. Matched NO_3^--N concentrations using the "Matched Parcels" method

3.1.1. Volumetric efficiency (e_V) in the Tatuanui bioreactor

Using the 2019 season monitoring data, the volumetric efficiency calculated for the Q1 and Q2 + Q3 sections were 0.82 (±0.08) and 0.56 (±0.05), respectively, and not effected by flow variation. The volumetric efficiency in the Q4 section of the bioreactor varied linearly with flow ($e_V = 0.04182*Q + 0.09135$, where Q is flow in L min^{-1}; $R^2 \approx 1.00$), i.e. effective pore volume ($V_{eff} = e_V \times$ saturated pore volume) increases

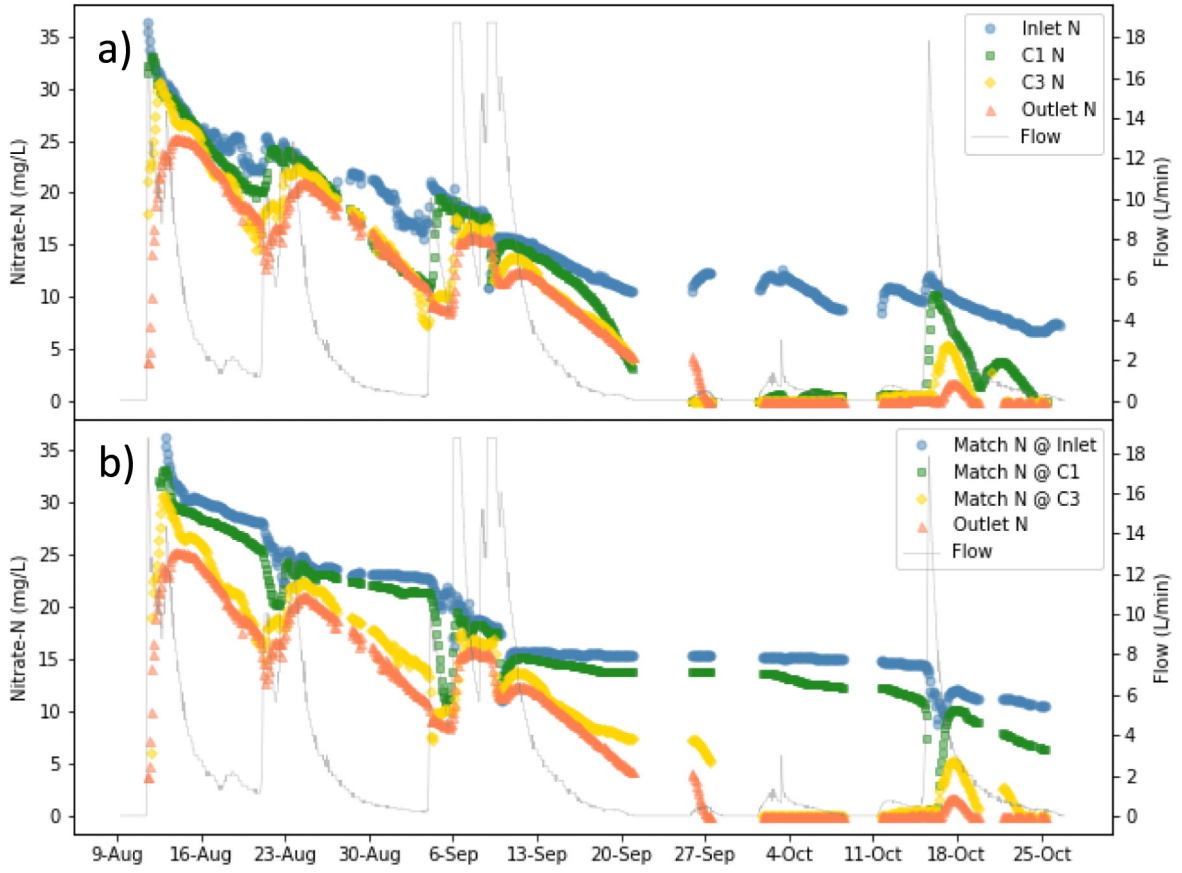

Fig. 3. Time series of nitrate concentrations at different locations along the length of the Tatuanui bioreactor a) as measured by the sensor, and b) lag time-adjusted (except outlet concentrations) during the 2019 drainage season.

with increasing flow. The saturated pore volume was based on total porosity (ϕ_t) and variable saturated volume. When considering only Inlet and Outlet nitrate peaks, the overall bioreactor volumetric efficiency was 0.54 (±0.10). According to Persson et al. (1999), volumetric efficiency can be categorised into three groups: good ($e_V > 0.75$), satisfactory ($0.5 < e_V \leq 0.75$), and poor ($e_V \leq 0.5$). The results show that the Tatuanui bioreactor has at least a satisfactory volumetric efficiency, except in the last quarter section (Q4) during low flows as discussed later (Section 4.1).

As the shortened 2018 season dataset did not allow for determining separate volumetric efficiencies due to lack of suitable discrete NO_3^--N peaks travelling through the bioreactor, the 2019 volumetric efficiency values were used for this 2018 period as well. This approach is reasonable given the drainable porosities for the bioreactor measured at the end of these two seasons were comparable, 0.45 in 2018 (Rivas et al., 2020b) and 0.50 in 2019 (data not shown).

Based on flow and volumetric efficiencies, the range of calculated hydraulic residence times (HRTs) in the 2018 season (59–408 h) was narrower compared to the range of HRTs in the 2019 season (27–510 h) (Supplementary table ST1). This is probably because the high-frequency monitoring was conducted in the later part of the 2018 season compared to the full 2019 season monitoring. The ranges of HRTs in the various sections along the length of the bioreactor are provided as a supplementary material (SF1). Longest HRTs observed in the Q2 + Q3 section in both seasons are attributed to the greater effective pore volume than the other sections.

3.1.2. Lag time-adjusted NO_3^--N concentrations

The NO_3^--N concentrations along the centreline as measured by the optical sensor and adjusted to account for the lag time are shown in Figs. 2 and 3 for the 2018 and 2019 seasons, respectively. The time series of NO_3^--N concentrations at all monitored locations, including the wells near the edge, in shallow and deep locations, within the bioreactor are provided as supplementary materials (SF2 and SF3). This complete data set was used in the transport modelling discussed in Section 3.3.2 below.

In both measurement campaigns, a decreasing trend in NO_3^--N concentrations was observed in the input tile drainage entering the bioreactor through the drainage season. Figs. 2a and 3a show the time series of measured NO_3^--N concentrations at the Inlet, two wells along the centreline of the bioreactor (C1 and C3), and Outlet during the two drainage seasons (2018 and 2019). Data from the well C2 along the centreline were not included in either year of this study due to unreliable NO_3^--N concentrations resulting from rodent damage to sample tubing in 2019. Gaps in the 2018 data series were due to the fouling of the sensor cuvette resulting in data being excluded; in 2019, NO_3^--N concentration data at no flow conditions were also excluded. The overall trend of decreasing NO_3^--N input through the drainage seasons indicates the gradual depletion of the soil NO_3^--N pool that is contributing into the drainage waters during the season (Barkle et al., 2021). This also explains the much higher NO_3^--N concentrations at the beginning of the 2019 drainage season in early August, compared to the beginning of the high-frequency monitoring in the 2018 season which started midway through the actual drainage season. Short-duration NO_3^--N peaks were observed throughout the season, reflecting the flushing out of nitrate generated in the most biologically active topsoil with higher flows, due to rainfall events (Liu et al., 2020b).

Decreasing NO_3^--N concentrations along the length of the bioreactor (i.e., from Inlet to Outlet) are also evident in both seasons (Figs. 2a and 3a), reflecting the nitrate reduction in the bioreactor. The decreasing average NO_3^--N concentrations at the Inlet, wells C1 and C3, and Outlet in the 2018 and 2019 seasons are provided in Tables 1 and 2, respectively. This decrease in NO_3^--N concentrations along the length of the bioreactor is visually more evident when concentrations were adjusted for the lag time (Figs. 2b and 3b; Tables 1 and 2). The importance of accounting for the lag time between locations is particularly evident during periods with low or intermittent flows, e.g. in September 2019. The lag-adjusted time series consistently show a reduction in concentrations from Inlet to Outlet (Tables 1 and 2).

3.2. Comparison of RR computed for the whole bioreactor using high- and low-frequency monitoring data

3.2.1. Comparison with using low-frequency NO_3^--N concentrations not accounting for the time lag

Considering that the usual practice in measuring the performance of bioreactors involves concurrent monitoring at inlet and outlet only, our results focused on comparing RR for the whole bioreactor using high-frequency NO_3^--N concentrations (2-hourly interval) and flows (5-minute interval). Monitoring on this frequency allows the lag time to be considered and RR determined on a high temporal basis and compared with concurrent RR calculated only using NO_3^--N concentrations and flow measured at low frequencies (e.g., only considering measurements at 6-, 12-, 24-hourly intervals). We did not include in the comparison the estimates of RR based on weekly frequency due to the relatively short drainage monitoring periods resulting in few data points, which would result in much lower equivalent sample sizes (n_e) with autocorrelation compensation.

Using the high-frequency 2019 data, the RRs were determined using NO_3^--N measurements only from 2-hourly and 6-, 12-, and 24-hourly intervals for the same monitoring period. The resulting average RRs (mean ± stdev) were 0.91 (±0.48), 0.62 (±0.83), 0.60 (±0.83), and 0.63 (±0.84) g-N m^{-3} day^{-1}, respectively (Fig. 4a). The RRs at 2-hourly interval, which accounted for the lag time, were significantly higher ($p < 0.05$) than the concurrent RRs measured with low-frequency data (i.e., NO_3^--N measurements at 6-, 12-, and 24-hourly intervals) and not accounting for the lag time. However, no significant difference ($p > 0.05$) was found among concurrent RRs obtained with lower-frequency data.

3.2.2. Comparison with using low frequency, but matched concentrations (i.e., accounting for lag time)

Interestingly, when lag time was accounted for in calculating RR even with low-frequency monitoring, there was no significant difference ($p > 0.05$) in RRs calculated with different sampling frequencies ranging from 2-hourly to 24-hourly interval (Fig. 4b). Average RRs (mean ± stdev) between Inlet and Outlet using matched concentrations at 2-, 6-, 12-, and 24-hourly intervals were 0.91 (±0.48), 0.92 (±0.48), 0.93 (±0.41), and 0.92 (±0.42) g-N m^{-3} day^{-1}, respectively.

3.3. Spatiotemporal variability of nitrate removal rates (RR) in the Tatuanui bioreactor

3.3.1. Variability along the centreline of the bioreactor

The variability in nitrate RRs with time in the 2018 and 2019 seasons is shown in Figs. 5 and 6, whereas the spatial variability among sections is shown in Fig. 7. Early in the monitored 2018 season, RRs were largely comparable among the different sections of the bioreactor (Fig. 5). However, at the latter part of the monitoring period when lower NO_3^--N concentrations were observed, differences in RR among the sections were more apparent. During this latter part of the season, higher RRs were observed in the Q2 + Q3 section, followed by essentially similar RRs in the Q1 and Q4 sections. This is also generally reflected in the range of RR among the three sections over the entire monitoring period shown in Fig. 7a. With an average RR of 0.86 (±0.19) g-N m^{-3} day^{-1}, the Q2 + Q3 section had higher RRs than in sections Q1 and Q4 in 2018, with average RRs of 0.58 (±0.13) and 0.58 (±0.33) g-N m^{-3} day^{-1}, respectively. However, the differences in RR between sections were not statistically significant, which could be attributed to the very low equivalent sample sizes ($n_e < 6$, from original sample sizes of n = 220–250) resulting from high autocorrelation ($\rho > 0.95$) in the RRs in each section.

In the analysed period of the 2019 season, predominantly higher RRs in the Q4 section were observed most of the season, except during low flows when the highest RRs were generally observed in the Q1 or Q2 + Q3 section (Figs. 6 and 7b). With an average RR of 1.3 (±1.3) g-

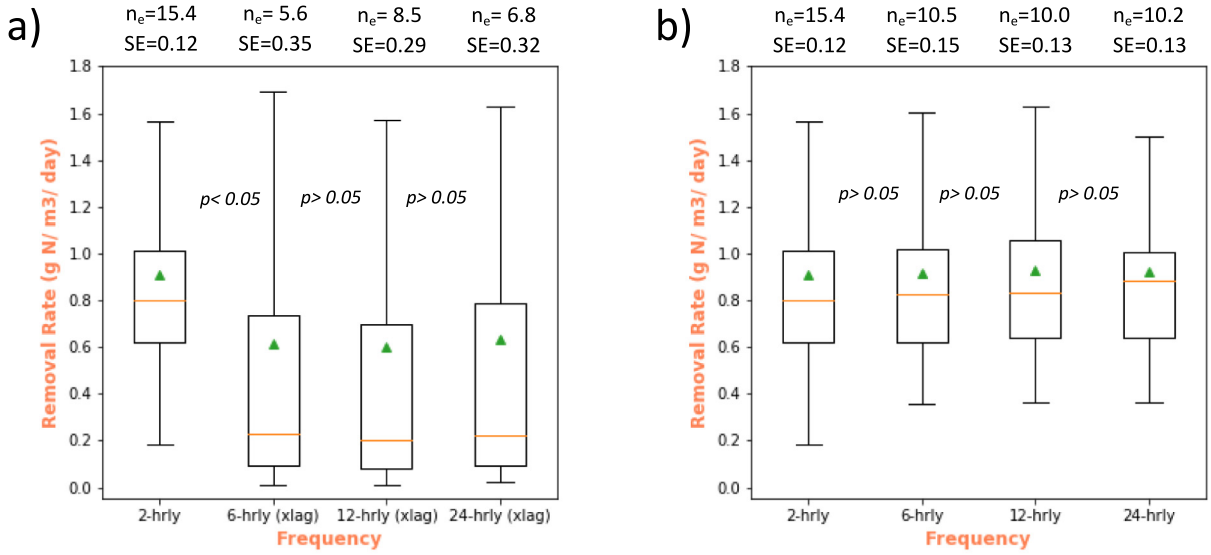

Fig. 4. Comparison of RR computed at different frequencies for the whole bioreactor during the 2019 season. a) 2-hourly interval accounts for the lag time, whereas other frequencies did not account for the lag time (xlag); b) all accounted for the lag time. Green triangles and the orange line in the box are the mean and median, respectively.

N m^{-3} day^{-1}, the Q4 section had higher RRs than the other sections, followed by the Q2 + Q3 section and then the Q1 section with average RRs of 0.90 (±0.54) and 0.81 (±0.57) g-N m^{-3} day^{-1}, respectively. While the differences in RR between Q1 and Q2 + Q3 and between Q2 + Q3 and Q4 were not statistically significant, section Q4 had statistically higher RRs ($p < 0.05$) than section Q1. With a range of ρ = 0.60–0.88, autocorrelation coefficients in the 2019 RR time series in the three sections were lower compared to the 2018 RRs and resulted in higher equivalent sample sizes (n_e = 30–112, from original sample sizes of n = 440–475).

In general, the average RR computed for the entire bioreactor (i.e., Inlet-Outlet) in the 2019 season (0.91 ± 0.48 g-N m^{-3} day^{-1}) was higher than in the 2018 season (0.71 ± 0.09 g-N m^{-3} day^{-1}) (Fig. 7), but the difference was not statistically significant. This could be attributed to the high standard error in the 2019 data (Fig. 7) and the high autocorrelation ($\rho > 0.90$) in the high-frequency data (frequency ≤ 2 h) resulting in small equivalent sample sizes, especially in the short 2018 monitoring. This result appears to indicate that in order to have meaningful statistical results in comparing removal rates calculated from high-frequency data (frequency ≤ 2 h), a substantially larger sample size is essential to compensate for the effect of the autocorrelation.

3.3.2. Variability across the bioreactor using data from all monitoring wells

3.3.2.1. Spatially variable k. The variability in the estimated k (in g-N m^{-3} day^{-1}) between each section, along the five flowlines of the bioreactor in 2018 and 2019 is shown in Fig. 8. The simple 1D transport model fitted the high frequency data very well, with nRMSE between measured and simulated NO_3^--N concentrations at 5.4 % and 4.9 % for years 2018 and 2019, respectively. There was a general pattern of decreasing k along the flow path, but removal dynamics differed significantly between the two drainage years. In 2018 k was always greater in P2, due to conditions favourable to denitrification as compared to other sections (Fig. 8a). While average DO concentrations at the Inlet were approx. 4 mg L^{-1}, DO concentrations at the beginning of P2 were low and on average <1 mg L^{-1} (Rivas et al., 2020a) (SF4a) and NO_3^--N concentrations were above 5 mg-N L^{-1} (SF2). On the other hand, nitrate limiting conditions were observed in the second half of the bioreactor (SF2). In the 2019 season, however, k appeared to peak closer to the Inlet with secondary peaks in the second part of the bioreactor (P3 & P4; Fig. 8b) potentially due to low or no flow zones near the Outlet resulting, for instance, in lower NO_3^--N concentrations at the exit end of section P4, as discussed earlier.

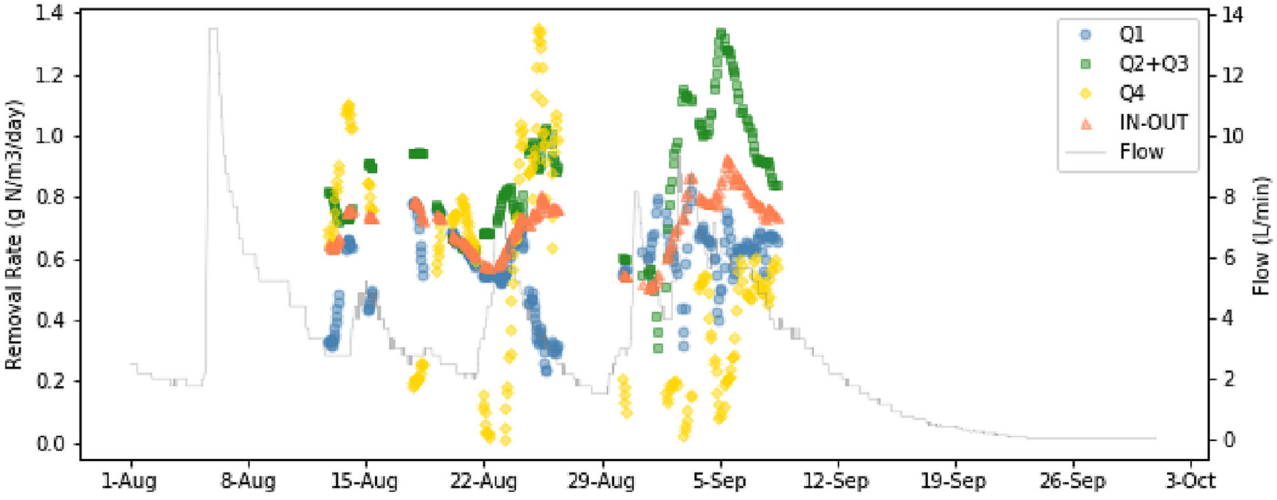

Fig. 5. Time series of nitrate removal rates based on one-hour sampling frequency at different sections of the bioreactor during the 2018 drainage season.

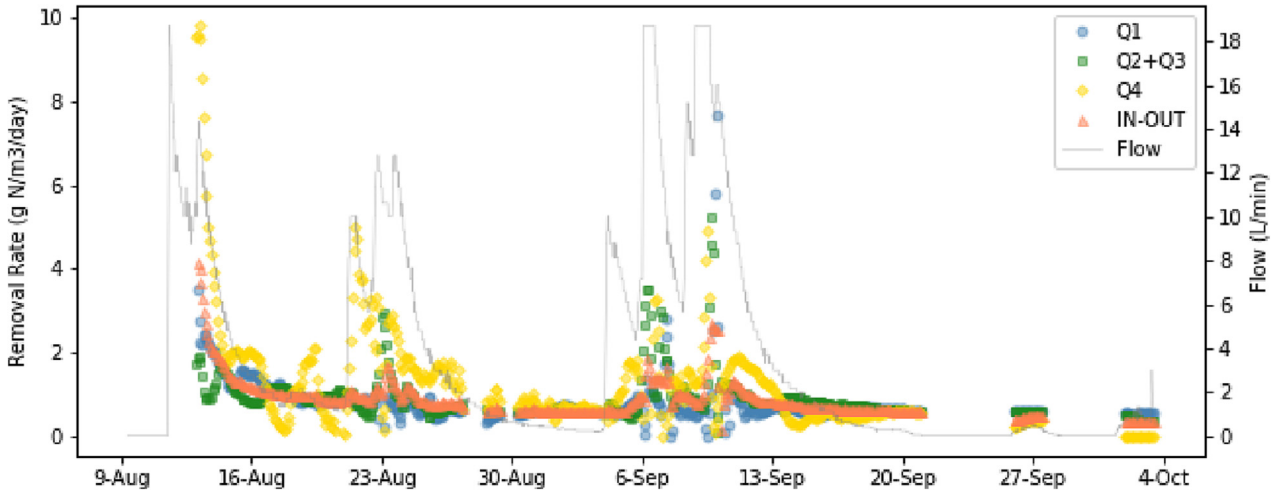

Fig. 6. Time series of nitrate removal rates based on two-hour sampling frequency at different sections of the bioreactor during the 2019 drainage season.

3.3.2.2. Maximum nitrate removal rates. The calibrated parameters of the model incorporating Michaelis-Menten kinetics are shown in Fig. 9. K_m was calibrated simultaneously with V_{max} using the nitrate limited 2018 data and then used to calibrate V_{max} for the 2019 season. The error term increased very slightly to 6.2 % and 5.4 % (from 5.4 % and 4.9 %) for years 2018 and 2019, respectively. However, the absolute small error indicates an excellent agreement between simulated and measured concentrations. The small error increase was expected as the number of model adjustable parameters decreased from 48 (Fig. 8) to 15 (Fig. 9).

For both years V_{max} was consistent across the five flow lines, ranging from 0.91 to 1.0 g-N m^{-3} day^{-1} and 0.71 to 0.75 g-N m^{-3} day^{-1} in 2018 and 2019, respectively.

4. Discussion

4.1. Hydrological dynamics in woodchip bioreactors

Estimates of volumetric efficiency (e_V), and consequently effective pore volumes (V_{eff}), of each quarter section of the bioreactor using the 2019 season data revealed the effectiveness of the different sections of the bioreactor.

Analysis for the Q1 section indicates that flow distribution in this section was very good, likely due to the use of a distribution header. This is supported by the apparent even distribution of flow between 0.5 m to 3.2 m (and even down to 5.9 m) from the Inlet header position in both seasons (SF2 and SF3).

The volumetric efficiency in the Q2 + Q3 section was 0.56, which indicates that the flow was satisfactorily distributed (SF2, SF3) in this section. The aspect ratio (length over width) of around 2 of the bioreactor could have contributed to the satisfactory volumetric efficiency in this section. This is because flows in bioreactors with higher aspect ratio were found to approximate piston flow due to increased dispersion across the narrower cross sections especially at higher velocities (Alcocer et al., 2012).

For the last section (Q4), the relationship between effective pore volume and flow indicates that the effective pore volume increased linearly with flow. At low flows, the effective pore volume in this section was smaller than the drainable pore volume, indicating non-uniform flow through this section of the bioreactor. For instance, only 0.2 of the calculated drainable pore volume (or 0.12 of total pore volume) of Q4 seemed active at a median flow of approx. 0.72 L min^{-1}. This apparent dead flow zone existing during low flows was likely occurring above the outlet collection pipe and could explain the unexpected low NO_3^--N concentrations in

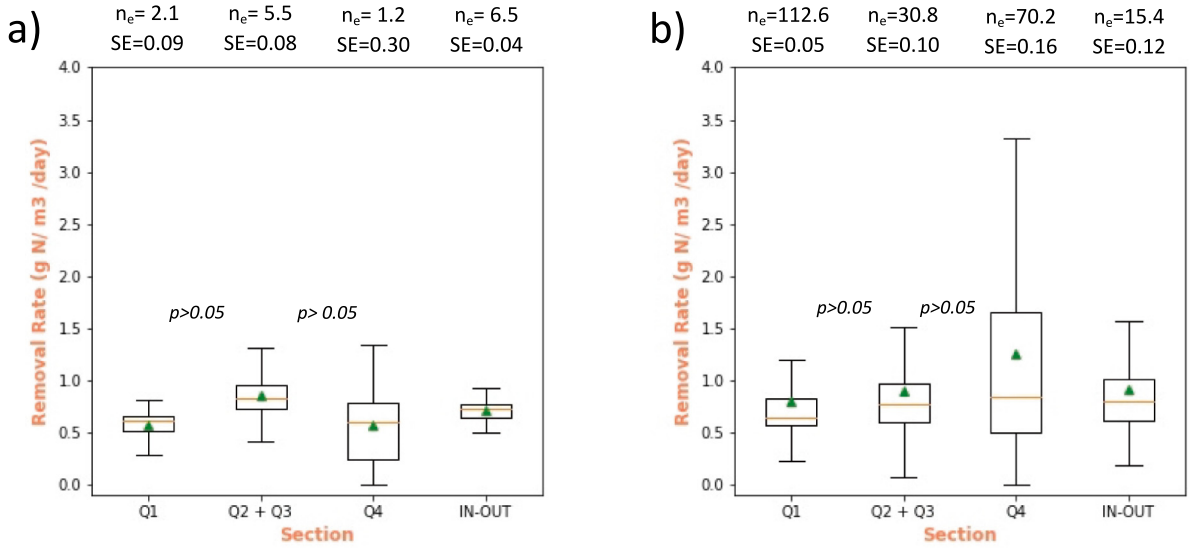

Fig. 7. Distribution of nitrate removal rates at different sections of the Tatuanui bioreactor during the a) 2018 and b) 2019 drainage seasons. Green triangles and the orange line in the box are the mean and median, respectively.

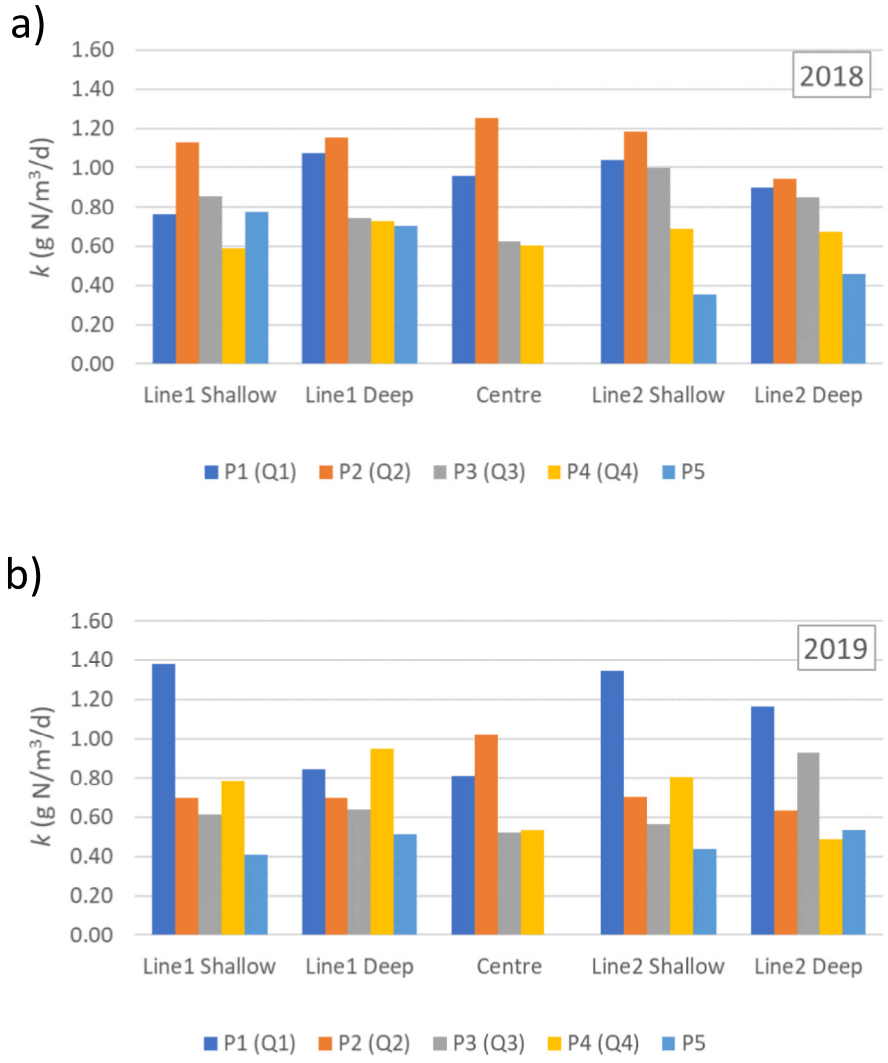

Fig. 8. Estimated zero-order nitrate treatment rates (k) at different sections of the Tatuanui bioreactor during the a) 2018 & b) 2019 seasons. P1–P5 are the five bioreactor sections along flowlines 1 & 2. Q1–Q4 are the four bioreactor sections in the centre line (see Fig. 1).

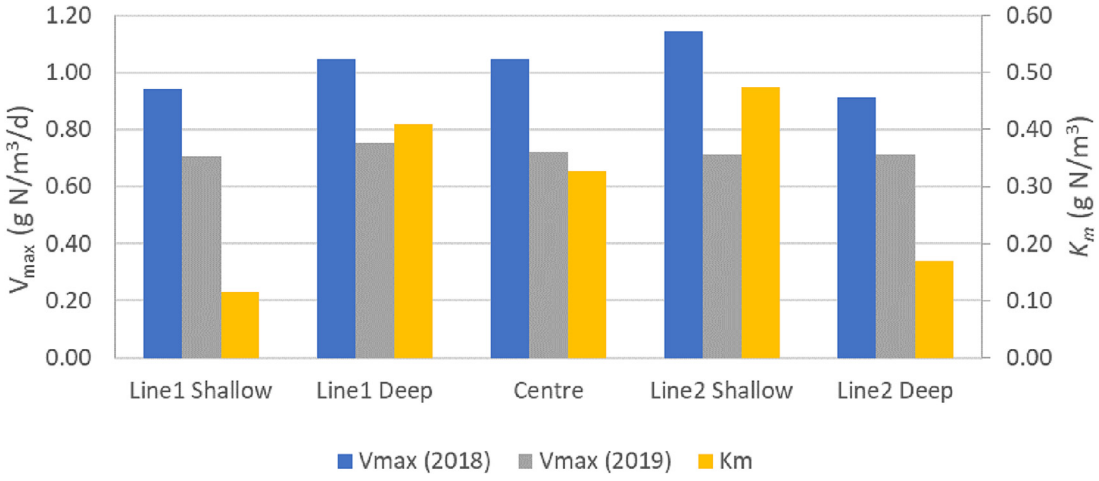

Fig. 9. Estimated maximum nitrate removal rates (V_{max}) and half saturation constants (K_m) at the five monitored flowlines of the Tatuanui bioreactor.

the shallow wells at row four (S4 and S8) (Fig. 1, SF2–SF3). Other studies have also observed preferential flows especially at lower flows (Alcocer et al., 2012).

The overall bioreactor e_V of 0.54 indicates that lag time estimates for the Tatuanui bioreactor based only on the total pore volume may not provide a reasonable approximation. Estimates using the drainable pore volume may provide a reasonable approximation of lag times. However, either of these two approaches would not have revealed the important insights on flow dynamics occurring in the bioreactor, especially with the significant changes in the active volume in the Q4 section of the bioreactor. Thus, for wide bioreactors (i.e., smaller length over width ratio) with elevated Inlet distribution header, larger dead volumes near the outlet may be expected at low flows.

4.2. Improved RR estimates using lag time-adjusted NO_3^--N concentrations from high-frequency monitoring

Our results demonstrate that, in drainage systems with highly dynamic flows, reducing the field sampling interval from the typical weekly to daily or even sub-daily intervals to calculate RR using the concurrent RR method may not result in achieving the accuracy of RR calculated based on 2-hourly measurements which take lag times into account. More measurements (count = 479) capturing the dynamics in NO_3^--N concentrations were involved in computing RR using the high-frequency data, in contrast to the low-frequency sampling (count = 156, 77, and 36 for 6-, 12-, and 24-hourly sampling interval, respectively).

Provided the lag time is accounted for, it appears that a daily (24-h) interval seems sufficient for obtaining an accurate measure of nitrate removal performance. However, highly accurate accounting for the lag time in the analysis of low-frequency data is challenging without the high-frequency data or alternatively multiple tracer tests covering the range of dynamic flow rates. It is acknowledged that it is challenging to identify and track NO_3^--N peaks in low-frequency data because a clear trend in NO_3^--N concentrations may not be apparent. Further analysis of the 2019 data (not shown) shows that using different sampling times for the same frequency interval (i.e., for the 6-, 12-, 24-hourly measurements) does not significantly affect the computed RR and the comparison and conclusions are still valid using different sampling times.

Using the high-frequency data and inverse 1D flow and transport modelling using spatially variable reaction (i.e., removal) rates at various sections of the bioreactor revealed that uniform reaction rates, often used for design purposes, significantly underestimate nitrate transformations at the first part of the bioreactor and significantly overestimate them near the outlet. This can have considerable implications for parameter transferability and comparisons of different designs when the bioreactor geometry and loading characteristics are not fully accounted for. Nitrate reduction kinetics follows a Michaelis-Menten kinetics model, which if incorporated in bioreactor design can better account for the transformation dynamics along a bioreactor. The non-uniform calibrated K_m values point out the need for more high-frequency datasets to better understand the K_m responses to highly dynamic loading conditions that are often expected in field applications.

4.3. Insights on the variability in nitrate removal processes within the woodchip bioreactor

The range and mean RR reported in this study are in the lower range of published RR values of field bioreactors: 0.01 to 22 g-N m^{-3} day^{-1} (Schipper et al., 2010b; Addy et al., 2016; Griessmeier et al., 2019; Manca et al., 2021). However, our results are generally comparable with RR in other bioreactors using the same woodchip material, i.e. *Pinus radiata* (Warneke et al., 2011c). There are several factors affecting RR including temperature, NO_3^--N mass loading (i.e., NO_3^--N concentrations and flow), hydraulic retention time, age of woodchips or electron donor source, and microorganisms (Bruun et al., 2016). Identifying the factors responsible for the relatively low RR compared with other studies is outside the scope of this study. Nevertheless, the most likely causes of this difference include the available carbon supply from the substrate (woodchips), denitrifier abundance and composition, and lower temperature (considering that drainage season occurs only during winter and spring as opposed to systems with generally year-round drainage). Soft wood materials, such as the pine wood used in this study, were found to have lower RR compared to other carbon sources (e.g., maize cobs, eucalyptus woodchips, saw dust, etc.) (Warneke et al., 2011c). This low RR could be due to the inferior amount of nitrite reductase genes (responsible for nitrite reduction) found in bioreactor barrels with pine wood, with positive relationship observed between RR and total nitrite reductase genes per unit of dry substrate (Warneke et al., 2011c). Low nitrite reductase could indicate the potential accumulation of nitrite in the bioreactor, which in turn could limit nitrate reduction (Glass et al., 1997). We were not able to compare the role of DOC on nitrate removal in our Tatuanui bioreactor with other studies due to the lack of published DOC data in the assessment of other field-scale bioreactors using other electron donor sources.

In terms of modelled nitrate removal rate, *k*, the trend of higher k near the Inlet appears in contrast to Fig. 7b where the highest removal rates were observed in the last quarter section of the bioreactor. The slight divergence in results could reflect the different datasets and analyses employed. In investigating the variability of nitrate RR along the centre line (Section 3.3.1), we used a larger dataset of the measured NO_3^--N concentrations compared to the 1D transport modelling which used the early part only of the monitoring period. Moreover, in Section 3.3.1 measured NO_3^--N concentrations were used between each section, whereas the modelling used the simulated concentrations produced from optimisation for determining *k*. This enabled determining *k* at sections Q2 and Q3, whereas Section 3.3.1 analysed the two quarters together as section Q2 + Q3, due to the measured data being unreliable at well C2. Calibrated *k* values ranged between 0.35 and 1.25 g-N m^{-3} day^{-1} in 2018, and between 0.41 and 1.38 g-N m^{-3} day^{-1} in 2019, and were generally higher in the 2019 season, in accordance with the removal rates presented in Section 3.3.1 (Fig. 7). The implications for bioreactor design and nitrate removal predictions are that loading and flow dynamics need to be carefully considered, while the variable hydrochemistry resulting in limiting conditions along the reactor need to be accounted for.

Moreover, the values of uniform maximum removal rate (V_{max}) obtained from modelling are lower than the limited available data reported in the literature. For example, Kouanda and Hua (2021) reported V_{max} of the order of 16.8–25.2 g-N m^{-3} day^{-1} at 22 °C and 1.68–5.04 g-N m^{-3} day^{-1} at 5 °C. The same reasons for the lower RR in the Tatuanui bioreactor provided in Section 3.3.1 are relevant here with respect to V_{max}. Moreover, in 2019 average V_{max} was 29 % lower than in 2018, which is also consistent with woodchip ageing. K_m was more variable across the flow lines, ranging between 0.12 and 0.47 g-N m^{-3}. Again these values were lower than those reported by Kouanda and Hua (2021) (1.19–2.60 g-N m^{-3}). K_m values have been considered as providing indications of the threshold NO_3^--N concentrations between zero-order and first-order reaction kinetics; meaning if concentrations are substantially higher than K_m, then the reaction is believed to be zero-order (Kouanda and Hua, 2021). The K_m values derived for the Tatuanui bioreactor agreed with reported threshold concentrations of 1.0 to 1.5 g-N m^{-3} reported by Bowman and Focht (1974). These results are also consistent with the observed nitrate limiting conditions affecting RR in the Q4 section of the bioreactor in 2018 (Section 3.3.1). Our findings suggest that bioreactor nitrate removal kinetics follow the MM model (Kouanda and Hua, 2021) and nitrate removal can be accurately quantified using V_{max} and K_m as substrate parameters.

The range of the Inlet-Outlet RRs in both seasons fell within the range of RRs in the three sections but does not reveal differences that occur between the sections. The differences in RR between sections reflect the different factors influencing nitrate removal. The following subsections discussed the various factors affecting nitrate removal processes along the length of the bioreactor, enhancing our understanding of these processes in woodchip bioreactors of similar configurations.

4.3.1. Partially oxic conditions near the Inlet causing lower nitrate removal

In both seasons, the average RRs observed in the first section (Q1) were lowest despite having the highest average NO_3^--N load at the Inlet of 2.4 and 5.8 g-N h^{-1} in 2018 and 2019, respectively, compared to other sections (Table 3). The low RR in this first section could be largely attributed to the partly oxic conditions in this section constraining the denitrification process (Rivett et al., 2008). Rivas et al. (2020a) reported average DO concentrations during the high-frequency monitoring period at the Inlet of 4.0 and 6.3 mg L^{-1} in 2018 and 2019, respectively (SF4). Whereas the average DO concentrations at about 35 % of the length of the bioreactor (second row of shallow and deep wells; no DO measurements done at C1 well at approx. 25 % of bioreactor length) during the same period were approximately 0.6 and 0.8 mg L^{-1} in 2018 and 2019, respectively. Several studies have suggested 2 mg L^{-1} as the upper DO limit for denitrification to occur, although denitrification has also been observed at higher concentrations up to 4 mg L^{-1} (Rivett et al., 2008; Thayalakumaran et al., 2008).

4.3.2. Nitrate-limiting conditions affecting nitrate removal performance especially near the Outlet

While earlier studies have shown that inflow NO_3^--N concentrations influenced RR (Addy et al., 2016), we focused this discussion on the impact of NO_3^--N loads (i.e., based on concentration and flow) on RR. Schmidt and Clark (2013) reported that in flow-through systems, like in our Tatuanui bioreactor, responses of denitrifiers appear to relate more strongly to the nitrate loading rate rather than concentration alone.

In 2018, the lower RR in the Q4 section compared to the Q2 + Q3 section (Section 3.3.1) could be attributed to nitrate limiting conditions in the Q4 section. An average NO_3^--N concentration of 2.4 mg-N L^{-1} and load of 0.7 g-N h^{-1} entered the Q4 section (Tables 1 and 3), whereas the average NO_3^--N load entering the Q2 + Q3 section was greater at 1.8 g-N h^{-1} (Table 3).

In the 2019 season, the average NO_3^--N load entering the Q4 section was relatively greater at 4.6 g-N h^{-1} (Table 3). This appears that, generally, the section was not nitrate limited resulting in greater average RR as compared to other sections, especially the Q1 section. However, during low flows in the second half of September to early October, RRs were very low (0.47 g-N m^{-3} day^{-1}; Fig. 3b) which could be attributed to nitrate limiting conditions with low NO_3^--N loads (0.45 g-N per 2-h parcels, or 0.22 g-N h^{-1}) entering this section (SF6). Moreover, the low flows also meant higher HRT, which would further lower the RR value.

These results indicate that, in bioreactors with greater length over width ratio (i.e., 'long' bioreactor) receiving highly dynamic drainage flows, it is likely for the latter part of the bioreactor to have unused nitrate removal capacity during low flow conditions. Accordingly, there is greater risk of developing highly reducing conditions, which is not desirable due to the production of greenhouse gases such as methane (Rivas et al., 2020b).

4.3.3. Availability of electron donor varies in the woodchip bioreactor limiting nitrate removal

Our analysis of the variability of RR and NO_3^--N in the drainage water shows that the nitrate removal performance of the Tatuanui bioreactor was largely influenced, not just by nitrate limitations (Section 4.3.2), but also by limitations in the availability of an electron donor (i.e. DOC).

For instance, in the 2018 season, the lower RR in the Q1 section – even with higher NO_3^--N loads – could be partly due to the lower DOC present in the first half of the bioreactor (in addition to the partially oxic conditions in this section) (Rivas et al., 2020b). The average DOC at the Inlet during the monitored period was 7.0 (±0.7) mg L^{-1}, which was significantly lower ($p < 0.05$) than the average DOC at the Outlet of 8.3 (±0.6) mg L^{-1} (Table 4).

Moreover, similar maximum RRs (approx. 1.4 g-N m^{-3} day^{-1}) were observed in the Q4 and Q2 + Q3 sections (SF7b) at different NO_3^--N loads: between 15 and 20 g-N day^{-1} in Q4 and between 80 and 95 g-N day^{-1} in Q2 + Q3 section. The comparable RR in the Q2 + Q3 section to the Q4 section despite the significantly higher NO_3^--N loads in the former could point to limitations in readily available electron donor (i.e., DOC). While there were no DOC measurements within the bioreactor in 2018, our measurements at C2 well in 2019 indicated increasing DOC along the length of the bioreactor (Table 4). The mean DOC concentration during the monitored period in the first half (i.e. average of DOC measured at Inlet and well C2) of 9.3 (±1.0) mg L^{-1} was significantly lower ($p < 0.05$) than average DOC of 12.4 (±2.4) mg L^{-1} in the second half (well C2 and Outlet) (Table 4). Limited studies on the relationship between RR and electron donor showed strong positive correlation between RR and DOC (either total or bioavailable only) (Warneke et al., 2011c; David et al., 2016). Thus, the nitrate removal performance of the Tatuanui bioreactor could be enhanced by supplementing with readily available electron donor, such as methanol or ethanol (Roser et al., 2018; Rivas et al., 2020b), but carbon-dosing would need to take into account the risk of negative side effects of creating highly reduced conditions.

4.3.4. Influent hydrology and hydrochemistry dictates the nitrate removal performance of field woodchip bioreactors

This study revealed the highly variable RRs, temporally and spatially, in a field-scale bioreactor operating under natural environmental conditions. As discussed above, several factors affect this variability but the importance

Table 3
Descriptive statistics of nitrate-N load (g-N h^{-1}) at different locations in the Tatuanui bioreactor measured in a) 2018 partial drainage season, and b) 2019 drainage season.

a) 2018 (g-N h^{-1})				
Statistic	Matched Inlet	Matched C1	Matched C3	Outlet
Mean	2.37	1.77	0.65	0.52
Median	2.16	1.33	0.52	0.38
Max	6.02	4.52	1.84	1.67
Min	0.95	0.68	0.10	0.04
Stdev	1.19	0.98	0.51	0.47
Cumulative (kg)	0.65	0.49	0.18	0.14
b) 2019 (g-N h^{-1})				
Statistic	Matched Inlet	Matched C1	Matched C3	Outlet
Mean	5.75	5.36	4.57	4.17
Median	3.10	2.96	2.51	2.30
Max	28.73	26.85	24.59	19.06
Min	0.06	0.05	0.00	0.00
Stdev	6.33	5.99	5.37	4.83
Cumulative (kg)	5.52	5.16	4.40	4.03

Table 4
Descriptive statistics of DOC concentrations (mg L^{-1}) at the Inlet, Middle Well, and Outlet in the Tatuanui bioreactor measured in a) 2018 partial drainage season, and b) 2019 drainage season, measured weekly to fortnightly. Inlet and Outlet data from samples collected automatically by ISCO samplers.

a) 2018			
Statistic	Inlet	Middle well	Outlet
Mean	6.76	–	10.66
Median	6.45	–	8.80
Max	11.30	–	53.90
Min	4.50	–	7.00
Stdev	11.30	–	6.39
Count	84	–	84
b) 2019			
Statistic	Inlet	Middle well[a]	Outlet
Mean	8.95	10.64	15.54
Median	8.80	9.25	12.10
Max	11.10	18.00	67.70
Min	6.90	8.25	8.30
Stdev	1.22	3.42	10.78
Count	35	7	39

[a] Middle well data from manual samplings.

of nitrate loading and DOC availability could not be overemphasised, particularly in bioreactors receiving drainage with highly dynamic flows and chemistry. The dependency on nitrate loading is reflected in that the nitrate removal dynamics in the bioreactor can be described by Michaelis-Menten kinetics (Section 4.2).

The effect of influent loading on the performance of bioreactors is also reflected in the greater RR in the 2019 season compared to the monitored period in the 2018 season, although the difference was not statistically significant due to very low 2018 equivalent sample size after compensating for autocorrelation. This greater RR could be attributed to the generally higher NO_3^--N concentrations and loads in the 2019 season (Tables 1–3) as NO_3^--N concentrations and/or loads have been found to influence nitrate removal rates (Schmidt and Clark, 2013; Addy et al., 2016). Consistent with this, the RR reported in this study represent actual RR achieved in the field and not the potential laboratory-based RR, where NO_3^--N concentration is controlled and carbon (i.e., DOC) may not be limiting (especially with fresh woodchips). For instance, our results showed that the Tatuanui bioreactor has the potential to remove nitrate at a rate of about 10 g-N m^{-3} day^{-1} (Figs. 6 and SF8). This was observed in the Q4 section of the bioreactor during the early part of the 2019 season (13 Aug) when nitrate and available DOC were apparently not limited (SF10b). The generally high DOC concentrations observed at the Outlet at the start of each season, with the bioreactor drained in between seasons, reflects the effect of drying and rewetting cycles on DOC availability (Maxwell et al., 2019). However, this apparent nitrate removal potential was rarely reached due to a combination of nitrate and/or C limiting conditions. The potential RR of approx. 10 g-N m^{-3} day^{-1} observed in 2019 was not reached in the partial 2018 season when high-frequency monitoring was undertaken with NO_3^--N concentrations at the Inlet below 10 mg L^{-1} (Figs. 2 and SF7b, Table 3), N loads were around 6 g-N h^{-1} (Table 3, SF5) and DOC concentrations at the Outlet (8.3 ± 0.6 mg L^{-1}) were lower than earlier in the season (SF10a).

These results underline the challenges of ascertaining, before a bioreactor is built, how much nitrate removal (especially in terms of RR) can be expected from a bioreactor operating under field conditions. This uncertainty may be reduced by collecting an increased amount of field flow and concentration data or producing reasonable synthetic (say 5–10 years) NO_3^--N loads that can be used in estimating the NO_3^--N loads to the bioreactor. Moreover, information on DOC availability from woodchip and supplemental sources is also important to have an idea of carbon limiting conditions.

4.4. Considerations for improving effectiveness of woodchip bioreactors

Our findings on volumetric efficiencies, e.g. concerning design characteristics encouraging piston flow conditions and minimising the occurrence of dead zones, seem to favour designs with greater aspect ratio (length over width), especially in high flow conditions. However, this may result in nitrate removal that is sub-optimal during low flows as our results showed nitrate limiting conditions in the latter part of the bioreactor indicating unused potential for removal. This greater aspect ratio may also result in an increase in highly reduced conditions, which may have negative side effects such as methane and/or hydrogen sulphide production (Rivas et al., 2020b). On the other hand, bioreactors with short aspect ratio may be more vulnerable to being affected by preferential flow paths, which are high conductivity paths connecting the Inlet and the Outlet. Therefore, a balance between volumetric efficiency and nitrate removal performance needs to be considered when designing a bioreactor. This requires a good understanding of the dynamics of the drainage flow and hydrochemistry, as essential for understanding uncertainties in expected nitrate removal at the design stage. For instance, the high nitrate loading at the beginning of a drainage season and variable loads throughout the season, common in NZ temperate pasture lands, may require that a larger bioreactor is desirable early in the season and a smaller bioreactor in operation in the latter part of the season or at low flows. This may be achieved by having two smaller bioreactors installed in parallel with the second bioreactor treating overflows from the Inlet of the first bioreactor. Ultimately, the decision for bioreactor design and sizing would be influenced by the costs and desired benefits.

5. Conclusions

This work demonstrated the benefits of high-frequency monitoring data of nitrate concentrations at multiple locations in a bioreactor by improving the quantification of nitrate removal performance and enhancing the understanding of removal processes. Using an approach which accounts for the lag time through the bioreactor, we quantified the volumetric inefficiencies within the bioreactor, revealing the dynamics of dead zones within the bioreactor.

Regardless of the monitoring interval, we showed that nitrate removal rates cannot be reliably quantified without accounting for the lag time and effective pore volume, especially in systems which experience highly variable inflows. To evaluate the lag time correctly, high-frequency monitoring is essential.

The spatiotemporal variability in nitrate removal rates revealed the influence of flow and hydrochemistry on denitrification along the length of the bioreactor. We showed that a Michaelis-Menten formulation can describe the RR kinetics in the Tatuanui bioreactor. Additionally, the study showed that an optimal length over width ratio of the bioreactor is important to maximise the bioreactor's performance.

Our assessment of nitrate removal performance with high-frequency data were conducted for a single bioreactor. It would be useful to apply these methodologies for monitoring and quantifying the nitrate removal performance of other bioreactors in different environmental settings and configurations to obtain more information on the benefits of high-frequency monitoring. This study employed high-frequency time series data which exhibited a strong autocorrelation, significantly reducing the equivalent sample sizes. Thus, in order to maintain sufficient statistical resolving power, it is important to plan for an appropriately large sample size.

The authors contend that the insights gained from this study would be helpful to inform future designs for more effective bioreactors.

CRediT authorship contribution statement

A. Rivas: Conceptualization, Methodology, Investigation, Data curation, Formal analysis, Project administration, Visualization, Writing – original draft, Writing – review & editing. **G. Barkle:** Funding acquisition, Conceptualization, Methodology, Investigation, Formal analysis, Project administration, Writing – review & editing. **T. Sarris:** Methodology, Software, Formal analysis, Visualization, Writing – original draft, Writing – review & editing. **J. Park:** Methodology, Software, Formal analysis, Writing – review & editing. **A. Kenny:** Methodology, Software, Formal analysis, Visualization, Writing – original draft, Writing – review & editing. **B. Maxwell:** Methodology, Investigation, Data curation. **R. Stenger:** Funding acquisition, Supervision, Project administration, Writing – review & editing. **B. Moorhead:** Methodology, Investigation, Data curation. **L. Schipper:** Supervision, Resources, Writing – review & editing. **J. Clague:** Investigation, Project administration.

Data availability

Data will be made available on request.

Declaration of competing interest

The authors declare that they have no known competing financial interests or personal relationships that could have appeared to influence the work reported in this paper.

Acknowledgements

This work was carried out under the MBIE-funded programmes "Enhanced Mitigation of Nitrate in Groundwater" led by ESR and

“Doubling On-farm Diffuse Pollution Mitigation” led by NIWA. We gratefully acknowledge the co-operation of the landowners, the Mourits family. We wish to acknowledge the three anonymous reviewers for their helpful feedback that greatly improved this manuscript.

Appendix A. Supplementary data

Supplementary data to this article can be found online at https://doi.org/10.1016/j.scitotenv.2023.163289.

References

Addy, K., Gold, A.J., Christianson, L.E., David, M.B., Schipper, L.A., Ratigan, N.A., 2016. Denitrifying bioreactors for nitrate removal: a meta-analysis. J. Environ. Qual. 45, 873–881.

Alcocer, D.J.R., Vallejos, G.G., Champagne, P., 2012. Assessment of the plug flow and dead volume ratios in a sub-surface horizontal-flow packed-bed reactor as a representative model of a sub-surface horizontal constructed wetland. Ecol. Eng. 40, 18–26.

Barkle, G., Stenger, R., Moorhead, B., Clague, J., 2021. The importance of the hydrological pathways in exporting nitrogen from grazed artificially drained land. J. Hydrol. (Amsterdam) 597, 126218.

Birgand, F., Aveni-Deforge, K., Smith, B., Maxwell, B., Horstman, M., Gerling, A.B., Carey, C.C., 2016. First report of a novel multiplexer pumping system coupled to a water quality probe to collect high temporal frequency in situ water chemistry measurements at multiple sites. Limnol. Oceanogr. Methods 14, 767–783.

Bowman, R., Focht, D., 1974. The influence of glucose and nitrate concentrations upon denitrification rates in sandy soils. Soil Biol. Biochem. 6, 297–301.

Bruun, J., Hoffmann, C.C., Kjaergaard, C., 2016. Nitrogen removal in permeable woodchip filters affected by hydraulic loading rate and woodchip ratio. J. Environ. Qual. 45, 1688–1695.

Cameron, S.C., Schipper, L.A., 2012. Hydraulic properties, hydraulic efficiency and nitrate removal of organic carbon media for use in denitrification beds. Ecol. Eng. 41, 1–7.

Cameron, S.G., Schipper, L.A., 2011. Evaluation of passive solar heating and alternative flow regimes on nitrate removal in denitrification beds. Ecol. Eng. 37, 1195–1204.

Christianson, L., Bhandari, A., Helmers, M., Kult, K., Sutphin, T., Wolf, R., 2012. Performance evaluation of four field-scale agricultural drainage denitrification bioreactors in Iowa. Trans. ASABE 55, 2163–2174.

Christianson, L., Helmers, M., Bhandari, A., Moorman, T., 2013. Internal hydraulics of an agricultural drainage denitrification bioreactor. Ecol. Eng. 52, 298–307.

Christianson, L.E., Cooke, R.A., Hay, C.H., Helmers, M.J., Feyereisen, G.W., Ranaivoson, A.Z., McMaine, J.T., McDaniel, R., Rosen, T.R., Pluer, W.T., Schipper, L.A., Dougherty, H., Robinson, R.J., Layden, I.A., Irvine-Brown, S.M., Manca, F., Dhaese, K., Nelissen, V., von Ahnen, M., 2021. Effectiveness of denitrifying bioreactors on water pollutant reduction from agricultural areas. Trans. ASABE 64, 641–658.

Daughney, C., Reeves, R., 2005. Definition of hydrochemical facies in the New Zealand National Groundwater Monitoring Programme. J. Hydrol. 44, 105–130.

David, M.B., Gentry, L.E., Cooke, R.A., Herbstritt, S.M., 2016. Temperature and substrate control woodchip bioreactor performance in reducing tile nitrate loads in east-Central Illinois. J. Environ. Qual. 45, 822–829.

Elgood, Z., Robertson, W.D., Schiff, S.L., Elgood, R., 2010. Nitrate removal and greenhouse gas production in a stream-bed denitrifying bioreactor. Ecol. Eng. 36, 1575–1580.

Etheridge, J.R., Birgand, F., Osborne, J.A., Osburn, C.L., Burchell, M.R., Irving, J., 2014. Using in situ ultraviolet-visual spectroscopy to measure nitrogen, carbon, phosphorus, and suspended solids concentrations at a high frequency in a brackish tidal marsh. Limnol. Oceanogr. Methods 12, 10–22.

Ghane, E., Fausey, N.R., Brown, L.C., 2014. Non-darcy flow of water through woodchip media. J. Hydrol. 519, 3400–3409.

Ghane, E., Fausey, N.R., Brown, L.C., 2015. Modeling nitrate removal in a denitrification bed. Water Res. 71, 294–305.

Ghane, E., Feyereisen, G.W., Rosen, C.J., 2016. Non-linear hydraulic properties of woodchips necessary to design denitrification beds. J. Hydrol. 542, 463–473.

Ghane, E., Feyereisen, G.W., Rosen, C.J., 2019. Efficacy of bromide tracers for evaluating the hydraulics of denitrification beds treating agricultural drainage water. J. Hydrol. 574, 129–137.

Ghasemi, A., Zahediasl, S., 2012. Normality tests for statistical analysis: a guide for non-statisticians. Int. J. Endocrinol. Metab. 10, 486–489.

Glass, C., Silverstein, J., Oh, J., 1997. Inhibition of denitrification in activated sludge by nitrite. Water Environ. Res. 69, 1086–1093.

Griessmeier, V., Leberecht, K., Gescher, J., 2019. NO3 (-) removal efficiency in field denitrification beds: key controlling factors and main implications. Environ. Microbiol. Rep. 11, 316–329.

Halaburka, B.J., LeFevre, G.H., Luthy, R.G., 2017. Evaluation of mechanistic models for nitrate removal in woodchip bioreactors. Environ. Sci. Technol. 51, 5156–5164.

Hassanpour, B., Giri, S., Pluer, W.T., Steenhuis, T.S., Geohring, L.D., 2017. Seasonal performance of denitrifying bioreactors in the northeastern United States: field trials. J. Environ. Manag. 202, 242–253.

Helsel, D., Hirsch, R., 2002. Statistical Methods in Water Resources. Book 4, Hydrologica Analysis and Interpretation. USGS, p. 510.

Holm, S., 1979. A simple sequentially rejective multiple test procedure. Scand. J. Stat. 6, 65–70.

Husk, B.R., Anderson, B.C., Whalen, J.K., Sanchez, J.S., 2017. Reducing nitrogen contamination from agricultural subsurface drainage with denitrification bioreactors and controlled drainage. Biosyst. Eng. 153, 52–62.

Jaynes, D.B., Kaspar, T.C., Moorman, T.B., Parkin, T.B., 2008. In situ bioreactors and deep drain-pipe installation to reduce nitrate losses in artificially drained fields. J. Environ. Qual. 37, 429–436.

Jaynes, D.B., Moorman, T.B., Parkin, T.B., Kaspar, T.C., 2016. Simulating woodchip bioreactor performance using a dual-porosity model. J. Environ. Qual. 45, 830–838.

Kadlec, R., Wallace, S., 2009. Treatment Wetlands. CRC Press, Boca Raton, FL, USA.

Kouanda, A., Hua, G., 2021. Determination of nitrate removal kinetics model parameters in woodchip bioreactors. Water Res. 195, 116974.

Lepine, C., Christianson, L., Sharrer, K., Summerfelt, S., 2016. Optimizing hydraulic retention times in denitrifying woodchip bioreactors treating recirculating aquaculture system wastewater. J. Environ. Qual. 45, 813–821.

Liu, W., Maxwell, B.M., Birgand, F.P., Youssef, M.A., Chescheir, G.M., Tian, S., 2020a. Multipoint high-frequency sampling system to gain deeper insights on the fate of nitrate in artifically drained fields. J. Irrig. Drain. Eng. 146, 06019012.

Liu, W., Youssef, M.A., Birgand, F.P., Chescheir, G.M., Tian, S., Maxwell, B.M., 2020b. Processes and mechanisms controlling nitrate dynamics in an artificially drained field: insights from high-frequency water quality measurements. Agric. Water Manag. 232, 106032.

Manca, F., Wegscheidl, C., Robinson, R., Argent, S., Algar, C., De Rosa, D., Griffiths, M., George, F., Rowlings, D., Schipper, L., Grace, P., 2021. Nitrate removal performance of denitrifying woodchip bioreactors in tropical climates. Water 13, 3608.

Maxwell, B.M., Birgand, F., Schipper, L.A., Barkle, G., Rivas, A.A., Helmers, M.J., Christianson, L.E., 2020. High-frequency, in situ sampling of field woodchip bioreactors reveals sources of sampling error and hydraulic inefficiencies. J. Environ. Manag. 272, 110996.

Maxwell, B.M., Birgand, F., Schipper, L.A., Christianson, L.E., Tian, S., Helmers, M.J., Williams, D.J., Chescheir, G.M., Youssef, M.A., 2019. Drying-rewetting cycles affect nitrate removal rates in woodchip bioreactors. J. Environ. Qual. 48, 93–101.

Maxwell, B.M., Birgand, F., Smith, B., Aveni-Deforge, K., 2018. A small-volume multiplexed pumping system for automated, high-frequency water chemistry measurements in volume-limited applications. Hydrol. Earth Syst. Sci. 22, 5615–5628.

O'Shaughnessy, P., Cavanaugh, J.E., 2015. Performing T-tests to compare autocorrelated time series data collected from direct-Reading instruments. J. Occup. Environ. Hyg. 12, 743–752.

Persson, J., Somes, N.L.G., Wong, T.H.F., 1999. Hydraulics efficiency of constructed wetlands and ponds. Water Sci. Technol. 40, 291–300.

Pluer, W.T., Morris, C.K., Walter, M.T., Geohring, L.D., 2019. Denitrifying bioreactor response during storm events. Agric. Water Manag. 213, 1109–1115.

Pollock, D.W., 1994. User's Guide for MODPATH/MODPATH-PLOT, Version 3: A Particle Tracking Post-processing Package for MODFLOW, The US: Geological Survey Finite-difference Ground-water Flow Model.

Rice, E.W., Baird, R.B., Eaton, A.D., Clesceri, L.S., 2012. Standard Methods for the Examination of Water and Wastewater. American Public Health Association, American Water Works Association, Water Environment Federation 1496 pp.

Rivas, A., Barkle, G., Maxwell, B., Moorhead, B., Stenger, R., Schipper, L., Birgand, F., Clague, J., 2020a. Determining the spatial variability of nitrate removal in a woodchip bioreactor through high frequency monitoring at multiple locations. In: Christensen, C., Horne, D., Singh, R. (Eds.), Nutrient Management in Farmed Landscapes: 33rd Annual FLRC Workshop. Vol. 33. Farmed Landscapes Research Centre, Massey University, Palmerston North, New Zealand , pp. 1–11.. https://www.massey.ac.nz/~flrc/workshops/20/Manuscripts/Paper_Rivas_11_2020.pdf.

Rivas, A., Barkle, G.F., Stenger, R., Moorhead, B., Clague, J.C., 2020b. Nitrate removal and secondary effects of a woodchip bioreactor for the treatment of subsurface drainage with dynamic flows under pastoral agriculture. Ecol. Eng. 148, 105786.

Rivas, A., Singh, R., Horne, D., Roygard, J., Matthews, A., Hedley, M.J., 2017. Denitrification potential in the subsurface environment in the Manawatu River catchment, New Zealand: indications from oxidation-reduction conditions, hydrogeological factors, and implications for nutrient management. J. Environ. Manag. 197, 476–489.

Rivett, M.O., Buss, S.R., Morgan, P., Smith, J.W., Bemment, C.D., 2008. Nitrate attenuation in groundwater: a review of biogeochemical controlling processes. Water Res. 42, 4215–4232.

Roser, M.B., Feyereisen, G.W., Spokas, K.A., Mulla, D.J., Strock, J.S., Gutknecht, J., 2018. Carbon dosing increases nitrate removal rates in denitrifying bioreactors at low-temperature high-flow conditions. J. Environ. Qual. 47, 856–864.

Sarris, T.S., Burbery, L.F., 2018. Stochastic multi-objective performance optimization of an in-stream woodchip denitrifying bioreactor. Ecol. Eng. 124, 38–50.

Sarris, T.S., Close, M., Abraham, P., 2018. Using solute and heat tracers for aquifer characterization in a strongly heterogeneous alluvial aquifer. J. Hydrol. 558, 55–71.

Schipper, L.A., Cameron, S.C., Warneke, S., 2010a. Nitrate removal from three different effluents using large-scale denitrification beds. Ecol. Eng. 36, 1552–1557.

Schipper, L.A., Robertson, W.D., Gold, A.J., Jaynes, D.B., Cameron, S.C., 2010b. Denitrifying bioreactors—an approach for reducing nitrate loads to receiving waters. Ecol. Eng. 36, 1532–1543.

Schmidt, C.A., Clark, M.W., 2013. Deciphering and modeling the physicochemical drivers of denitrification rates in bioreactors. Ecol. Eng. 60, 276–288.

Thackston, E., Shields, F., Schroeder, P., 1987. Residence time distributions of shallow basins. J. Environ. Eng. 113, 1319–1332.

Thayalakumaran, T., Bristow, K.L., Charlesworth, P.B., Fass, T., 2008. Geochemical conditions in groundwater systems: implications for the attenuation of agricultural nitrate. Agric. Water Manag. 95, 103–115.

Wang, X., Frankenberger, J.R., Kladivko, E.J., 2003. Estimating Nitrate-N losses from subsurface drains using variable water sampling frequencies. Trans. ASAE 46.

Warneke, S., Schipper, L.A., Bruesewitz, D.A., Baisden, W.T., 2011a. A comparison of different approaches for measuring denitrification rates in a nitrate removing bioreactor. Water Res. 45, 4141–4151.

Warneke, S., Schipper, L.A., Bruesewitz, D.A., McDonald, I., Cameron, S., 2011b. Rates, controls and potential adverse effects of nitrate removal in a denitrification bed. Ecol. Eng. 37, 511–522.

Warneke, S., Schipper, L.A., Matiasek, M.G., Scow, K.M., Cameron, S., Bruesewitz, D.A., McDonald, I.R., 2011c. Nitrate removal, communities of denitrifiers and adverse effects in different carbon substrates for use in denitrification beds. Water Res. 45, 5463–5475.

Williams, M.R., King, K.W., Macrae, M.L., Ford, W., Van Esbroeck, C., Brunke, R.I., English, M.C., Schiff, S.L., 2015. Uncertainty in nutrient loads from tile-drained landscapes: effect of sampling frequency, calculation algorithm, and compositing strategy. J. Hydrol. 530, 306–316.

Zheng, C., Wang, P.P., 1999. MT3DMS: A Modular Three-Dimensional Multispecies Transport Model for Simulation of Advection, Dispersion and Chemical Reactions of Contaminants in Groundwater Systems; Documentation and User's Guide. US Army Corps of Engineers-Engineer Research and Development Center, Vicksburg, MS, p. 169 p.

Zwiers, F., von Storch, H., 1995. Taking serial correlation into account in tests of the mean. J. Clim. 8, 336–351.